

Contact angle hysteresis on random self-affine rough surfaces in Wenzel's wetting regime: Numerical study

Stanimir Iliev* and Nina Pesheva†

Institute of Mechanics, Bulgarian Academy of Sciences, Acad. G. Bonchev St. 4, 1113 Sofia, Bulgaria

Pavel Iliev‡

ETH Zurich, Computational Physics for Engineering Materials, CH-8093 Zurich, Switzerland



(Received 29 June 2022; accepted 8 February 2023; published 24 February 2023)

We present a numerical study of the advancing and receding apparent contact angles for a liquid meniscus in contact with random self-affine rough surfaces in Wenzel's wetting regime. Within the framework of the Wilhelmy plate geometry, we use the full capillary model to obtain these global angles for a wide range of local equilibrium contact angles and for different parameters that determine the self-affine solid surfaces: Hurst exponent, wave vector domain, and root-mean-square roughness. We find that the advancing and receding contact angles are single-valued functions that depend only on the roughness factor determined by the set of values of the parameters of the self-affine solid surface. Moreover, the cosines of these angles are found to depend linearly on the surface roughness factor. The relations between the advancing, the receding, and Wenzel's equilibrium contact angles are investigated. It is shown that for materials with self-affine surface structure, the hysteresis force is the same for different liquids and it depends only on the surface roughness factor. A comparison with existing numerical and experimental results is carried out.

DOI: [10.1103/PhysRevE.107.024802](https://doi.org/10.1103/PhysRevE.107.024802)

I. INTRODUCTION

Determining the hysteresis of the apparent equilibrium contact angle (CA) θ_{app} [1], which the free interface of a liquid forms with a solid surface, is an important problem of capillary theory in relation to wetting of real solid surfaces [2]. The latter are characterized by the presence of heterogeneity and/or roughness. The conditions for retention and spreading of the three-phase contact line (CL) are determined by the fact that the CL is in a metastable equilibrium state when the apparent CAs θ_{app} (measured experimentally) lie in a certain interval, determined by its lower and upper limits, which are called minimum and maximum CAs, respectively. These angles are known as receding θ_r (RCA) and advancing θ_a (ACA), and the difference between these angles is defined as CA hysteresis (CAH). For real solid surfaces θ_r and θ_a deviate from the actual equilibrium contact angle θ_{eq} , defined by the Young equation. For them, the conditions which determine the equilibrium of the CL are reduced to obtaining θ_r and θ_a as functions of the parameters of heterogeneity (chemical and/or physical) of the solid phase. It has to be noted that in the context of new research results, it is necessary to also consider the type of wetting regime defined by the presence (Cassie's regime) or absence (Wenzel's regime) of air bubbles formed during contact [3,4]. Therefore, the measured RCA and ACA depend on the equilibrium wetting regime.

The study of the CAH as a measure of the degree of liquid adhesion to a solid surface [1] in both wetting regimes with various manifestations of solid phase heterogeneity and roughness is highly relevant, and priority should be given to theoretical and experimental investigations of systems describing real and technologically important three-phase systems. The present study focuses on determining the angles θ_r and θ_a for a liquid in contact with random self-affine rough solid surfaces in Wenzel's wetting regime. Such self-affine rough surfaces describe well a number of real materials, e.g., granite, basalt, and others [5]. There are several experimental data sets for the CAH when a liquid is in contact in Wenzel's wetting regime with random rough surfaces, e.g., on aluminum sheets [6], on polymer surfaces [7], on abrasive papers [8], on polypropylene [9], and on paraffin wax surfaces [10]. These results are not sufficiently supported by theoretical considerations and cannot be compared to theoretical investigations, which are limited to the two-dimensional (2D) case and include studies of θ_{app} for a liquid in contact with random topographical substrates [11], self-affine rough surfaces [12], and fractal surfaces [13]. However, due to the reduced dimensionality, these studies do not take into account the “kink depinning” along the CL, which has a significant impact on the CAH as can be seen in Refs. [14–17]. This effect can be established only if the full three-dimensional (3D) system is considered in theoretical and numerical investigations. In these studies for periodic defects, after a rigorous analysis of the stick, slip, and jump motion of the CL, two different depinning regimes were identified. For Wilhelmy plate geometry (see Sec. II) in the first one, termed block case, the CL jumps in a single move from one row of defects to another and it can

*stani@imbm.bas.bg

†nina@imbm.bas.bg

‡pavelsiliev@gmail.com

be investigated through a 2D analysis. In the second or kink case, the CL passes from one row of defects to another row through a series of single jumps from one defect at a time. For the kink-depinning mechanism the CAH takes smaller values than for the block case. The block-depinning regime cannot be observed for random self-affine rough surfaces, due to the random distribution of the defects, and every CL jump can be considered as a kink-depinning case. A relevant question to be addressed is whether the CAH for periodic surfaces is smaller than that for random self-affine rough surfaces with an equal roughness factor r (defined as the ratio between the actual and the projected area of the surface). Since the random self-affine rough surfaces can be represented as Fourier series [see Eq. (3) below], one can in principle use an asymptotic approach [18,19] to obtain 3D solutions for the shape of the liquid free surface and determine the CAH. However, as our previous research has shown, these solutions are valid only for very small values of the roughness factor r , even for periodic surfaces. Moreover, the case of random self-affine rough surfaces would require hundreds of thousands of modes to be considered for the analytical approach, ruling out the use of asymptotic methods.

To this day the only feasible method for determining 3D equilibrium meniscus shapes is to solve numerically the full capillary model. David and Neumann (DN) [20] made an important step in this direction by calculating the CAH for the case when the curvature of the free surface is very small, i.e., when the Laplace equation for the shape of the equilibrium liquid interface can be linearized. Due to the above assumption, their results were limited to surfaces with very small roughness factor $r \leq 1.0065$ leading to a CAH magnitude of only 1–3 degrees. To determine the CAH on surfaces characterized by significantly greater values of r , it is necessary to obtain the equilibrium shapes of the liquid meniscus without restricting the magnitude of the liquid interface deformations. This is the objective of the present study, which is based on obtaining numerical 3D solutions in the framework of the full capillary model. It is a continuation of previous studies in which results were obtained for the structure and characteristics of the three-phase contact [21]. This investigation focused on the CL roughness exponent ζ , which is determined by the scaling of the root-mean-square width $w(l) \sim l^\zeta$ over the length scale l of the CL.

II. PROBLEM FORMULATION

We will study the CAH on random self-affine rough surfaces through numerical simulation based on the experimental procedure for measuring the receding θ_r and advancing θ_a CAs using the Wilhelmy plate method [22–24]. In this type of experiment, a vertical solid plate, partially dipped in a tank of liquid, is slowly withdrawing from or immersing in the liquid. Due to capillary force, the liquid forms a meniscus at the contact with the vertical plate. The fluid interface is assumed to be in equilibrium and for each position of the plate, θ_{app} can be determined by the capillary rise method or through the vertical component of the capillary force, acting on the CL L . The two methods give very similar results [25]. Here, we will obtain θ_{app} using the CL height h of the equilibrium state of the meniscus, averaged along the CL - $\langle h \rangle$ (where \langle

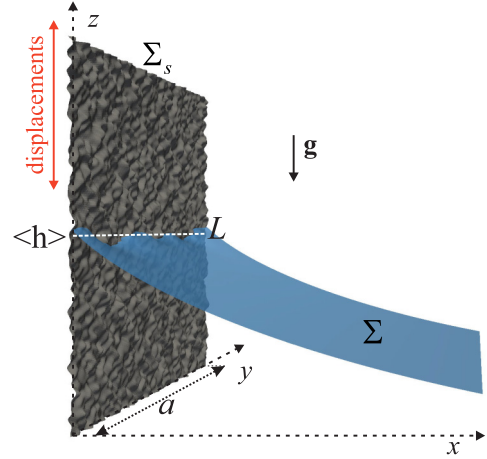


FIG. 1. Schematic image of a 3D meniscus, attached to a vertical rough solid plate.

denotes such a “horizontal” averaging). A schematic image of a 3D liquid meniscus attached to a vertical rough solid plate is shown in Fig. 1. The CA θ_{app} is defined as the angle which an equilibrium liquid meniscus with an average CL height $\langle h \rangle$ forms with a homogeneous vertical plane [20,26] and it is calculated using the following relation [27]:

$$\theta_{app} = \arcsin(1 - \langle h \rangle^2 / 2l_c^2), \quad (1)$$

where $l_c = \sqrt{\gamma / \rho g}$ is the capillary length, γ is the liquid-gas surface tension, ρ is the difference of the densities of the liquid in the tank and the ambient gas, and g is the gravity acceleration.

a. Advancing and receding contact angles. The advancing and receding contact angles θ_a and θ_r are determined from a series of equilibrium CLs L_i , $i = 1, 2, \dots$, obtained from a sequence of small vertical solid plate displacements with equal size Δ , simulating quasi-static motion of the solid plate into/from the liquid tank. If the averaged heights of the CLs L_i are $\langle h_i \rangle$ and the corresponding apparent contact angles are θ_{app}^i [Eq. (1)], then the CAs θ_a , θ_r are determined by averaging the angles θ_{app}^i when immersing or withdrawing the solid plate, respectively. One needs to consider results for $i > i_s$ (where s denotes slip) where i_s indexes the first CL L_{i_s} , for which $|\langle h_{i_s} \rangle - \langle h_{i_s+1} \rangle| \gg |\Delta|$. This criterion is based on the fact that changes of $\langle h_i \rangle$ equal to Δ when displacing the plate correspond to the stick regime, i.e., the CL remains adhered to the plate. The slip regime is established when the CL loses stability and starts sliding with respect to the plate, leading to significant changes in the CL height $\langle h_i \rangle$ between consecutive equilibrium states. Thus, it can be said that we take into account results for those $i > i_s$ for which a stick-slip motion of the CL has occurred.

b. Rough solid plate. In Cartesian coordinates, where the y axis is horizontal and the z axis is directed upward, and the plane $z = 0$ is chosen to coincide with the liquid level far from the vertical rough plate (as shown in Fig. 1), the solid plate Σ_s is described by the function $f(y, z)$, i.e., $\Sigma_s \equiv [f(y, z), y, z]$. We assume that $f(y, z)$ is periodic along the y - and z axes with period a , and that Σ_s is a random self-affine surface with roughness power spectrum $C(q) \sim q^{-2(H+1)}$, where

$q = \|(q_y, q_z)\|$ is the norm of the wave vector (q_y, q_z) , and H is the Hurst exponent. The surface is self-affine only in the finite region $q_0 < q < q_1$ defined by the long distance roll-off and short distance cutoff wave vectors q_0 and q_1 , analogous to real surfaces [5], and for the power spectrum we have

$$C(q) \sim \begin{cases} q^{-2(H+1)} & q > q_0 \\ C(q_0) & q \leq q_0 \end{cases}. \quad (2)$$

We obtain isotropic and self-affine functions $f(y, z)$, periodic in the y - and z directions, with the required properties defined in Eq. (2), by following the method suggested in Ref. [5]. In the square area $a \times a$, the function $f(y, z)$ is defined as

$$f(y, z) = \sum_{(q_y, q_z)} B(q) e^{i[q_y y + q_z z + \phi(q_y, q_z)]} \quad (3)$$

with wavelengths between $\lambda_1 = 2\pi/q_1$ and $\lambda_0 = 2\pi/q_0$.

In Eq. (3) $\phi(q_y, q_z)$ are random numbers uniformly distributed in the interval $[-\pi, \pi]$ and

$$B(q) = \sqrt{2R_q q^{-2(H+1)} / \sum_{(q_y, q_z)} \sqrt{q_y^2 + q_z^2}}, \quad (4)$$

where R_q is the root-mean-square of the surface roughness defined by

$$R_q = \sqrt{\langle f^2(y, z) \rangle_{yz}}. \quad (5)$$

By incrementally increasing or decreasing the plate position along the z axis by $i\Delta$, $i = 1, 2, \dots$, one can simulate withdrawing and immersing the plate from/into the pool of liquid. The parameters λ_0 , λ_1 , H , and R_q characterize the surface Σ_s and determine its roughness factor r . Note that the results for CAH as a function of r in Ref. [20] are presented without specifying the short-distance cutoff wavelength used for generating self-affine rough surfaces.

For the coordinate system and location of the rough solid plate Σ_s thus defined above (we assume Σ_s to be chemically homogeneous, i.e., the local CA θ_{eq} is the same at all points of the CL), the equilibrium of the liquid free-surface is determined by the local minimum of the free energy functional of the system $U(\Sigma)$:

$$U = \gamma \int_{\Sigma} d\Sigma + \gamma \cos \theta_{\text{eq}} \int_{\Sigma_{sl}} d\Sigma_{sl} + \int_V \rho g z dV, \quad (6)$$

where Σ_{sl} is the part of the plate surface, which is in contact with the liquid, and V is the liquid volume.

The local minimum of Eq. (6) is determined numerically using the same stepwise minimization algorithm from our previous studies on the structure of the contact line of the liquid meniscus in contact with a rough surface [16,21]. The liquid free surface Σ is approximated by a triangular mesh with $N_i \times N_j$ nodes, where N_i and N_j are the number of points in the x - and y directions, respectively. The mesh size constant Δ_L along the y direction is defined by $\Delta_L = a/N_j$, determining the discretization of the CL by $N_j - 1$ line segments. The parameters for the random self-affine rough surface used to obtain equilibrium meniscus solutions are identical to the ones in Ref. [21]. Since the results for the numerical simulations of DN are presented on the example of a system for which the

liquid used is water (this does not limit the generality of the results, as they can be presented in dimensionless form using the capillary length l_c), in view of easier comparison, the results obtained here for the same system are presented in dimensional units. Taking into account the periodicity of $f(y, z)$, it is sufficient to obtain a solution for the free liquid surface in the area between the planes $y = 0$ and $y = a$ by imposing periodic boundary conditions $z(x, 0) = z(x, a)$ at the boundaries of this area. In difference to the approximation of the CL used in DN, where the distance between the neighboring points of the mesh is $\Delta_L = 10 \mu\text{m}$, and $a = 1 \text{ mm}$, for the approximation of CL we use here $\Delta_L = 1 \mu\text{m}$ or $\Delta_L = 2 \mu\text{m}$, and our solutions are obtained for a between $a = 1 \text{ mm}$ and $a = 10 \text{ mm}$. We start the numerical algorithm with Σ having a CL, which adheres well to the rough solid surface and which has a constant height h_0 . There is no requirement for the value of h_0 , but it is desirable that it is close to $h_0 = l_c \sqrt{2(1 - \sin \theta_{\text{eq}})}$. For the presented below results for the CAH,

$$h_0 = l_c \sqrt{2(1 - \sin \theta_w)}, \quad \theta_w = \cos^{-1}(r \cos \theta_{\text{eq}}). \quad (7)$$

Thus, h_0 is the CL height of equilibrium liquid meniscus in contact with a vertical chemically homogeneous plate, forming a constant CA θ_w with the plate known as Wenzel's angle. The correctness of the obtained solution is monitored also by keeping track of the accuracy with which the points, approximating the surface Σ , satisfy the Laplace equation and the Young boundary condition. In this way it is ensured that the equilibrium meniscus states are obtained with high precision by the minimization method. This procedure is described comprehensively in Ref. [28]. The implementation of the numerical method has been tested for the Wilhelmy geometry where the liquid meniscus is in contact with doubly sinusoidal wavelike patterned surfaces [16] and it has been shown that for small roughness factors r the values obtained for the CAH are close to the asymptotically obtained predictions in Ref. [19].

As was shown and substantiated in detail by previous research on the wetting of rough surfaces in Wilhelmy geometry [16,21], for every equilibrium state with a CA θ_{eq} there is a *corresponding state* with an equilibrium CA $180^\circ - \theta_{\text{eq}}$. Thus, it is sufficient that numerical research is performed for the case $\theta_{\text{eq}} \leq 90^\circ$.

III. NUMERICAL RESULTS AND DISCUSSION

We study by means of numerical simulations how the RCA θ_r and ACA θ_a depend on the roughness factor r for different realizations of a self-affine rough surface, defined by the following values of the parameters characterizing the rough surfaces:

$$\begin{aligned} H &\in [0.1, 0.9], \quad \lambda_0 \in [200 \mu\text{m}, 1 \text{ mm}], \\ \lambda_1 &\in [25 \mu\text{m}, 50 \mu\text{m}], \quad R_q \in [1 \mu\text{m}, 6 \mu\text{m}], \end{aligned} \quad (8)$$

and for different values of the equilibrium CAs $\theta_{\text{eq}} \in [30^\circ, 90^\circ]$, which the liquid interface forms with the chemically homogeneous but rough solid surface. For a chosen set of parameter values (8), the surface roughness factor r is calculated by approximating the solid surface by a triangular mesh and summing up their surface areas. One has also to bear in mind that every function $f(y, z)$ depends on the specific

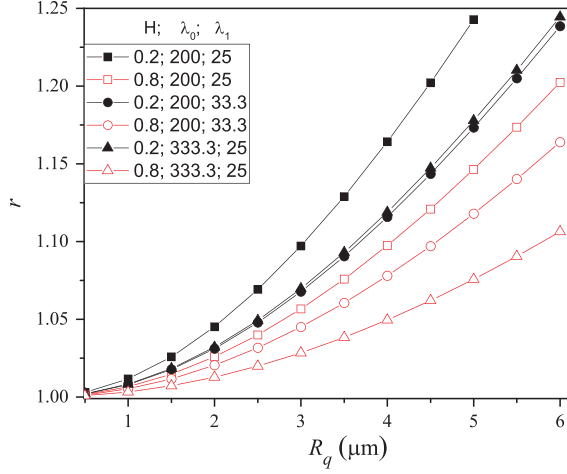


FIG. 2. Surface roughness factor r as a function of the standard deviation R_q for different sets of values of the rough surface parameters H , λ_0 (in μm), λ_1 (in μm).

realization of the random numbers $\phi(q_y, q_z)$, and therefore the obtained value of the roughness factor r is not uniquely determined by the values of the set of parameters (8). As a consequence of that, the obtained RCA and ACA as functions of r are not uniquely determined, but the values are very close for different realizations of $\phi(q_y, q_z)$, as shown by the numerical studies. The calculations for r reveal that when the values of three out of the four parameters in (8) are fixed, r decreases with increasing H and λ_0 , and increases with increasing λ_1 and R_q . Taking into account these dependencies, below we present results for two values of the Hurst exponent $H = 0.2$ and $H = 0.8$ (i.e., for small and large value of H). For each of them we present results for θ_r and θ_a for combinations of two different values of $\lambda_1 = 25 \mu\text{m}$, $\lambda_1 = 100/3 \mu\text{m}$ and $\lambda_0 = 200 \mu\text{m}$, $\lambda_0 = 1/3 \text{ mm}$. In Fig. 2 we present results obtained for the roughness factor ($r < 1.25$) as a function of R_q for the above values of the rough surface parameters. The calculations are made for values of $R_q = i0.5 \mu\text{m}$, $i = 1, 2, \dots$, and the results are shown by symbols connected by line segments. For each set of values for H , λ_0 , and λ_1 , solutions for the equilibrium shape of the liquid interface are obtained for these values of R_q , for which the free surface of the liquid Σ does not intersect the solid surface Σ_s in an interior for Σ area [4] (see Fig. 3). The nonintersection condition also depends on the value of θ_{eq} and more specifically, the largest value of R_q for which the condition is satisfied decreases with decreasing θ_{eq} . The numerical studies show that for $\theta_{\text{eq}} \in [30^\circ, 90^\circ]$, there is always a solution for θ_r and θ_a at least up to $R_q = 1.5 \mu\text{m}$, and the largest attainable R_q for θ_a is greater than that for θ_r . This follows from the fact that $\theta_r < \theta_a$ and that the probability of intersection of the two surfaces Σ and Σ_s increases with decreasing θ_{app} . As pointed out in the previous section, the calculation of the RCA θ_r and the ACA θ_a is preceded by obtaining θ_{app}^i at sequential displacements of the vertical solid plate on the basis of numerical solutions for the shape of the equilibrium interface Σ . Two representative results for the obtained sequences of θ_{app}^i when the plate is withdrawing and immersing are shown in Fig. 4. These results are obtained for a rough surface characterized by $H = 0.2$, $\lambda_0 = 200 \mu\text{m}$, $\lambda_1 =$

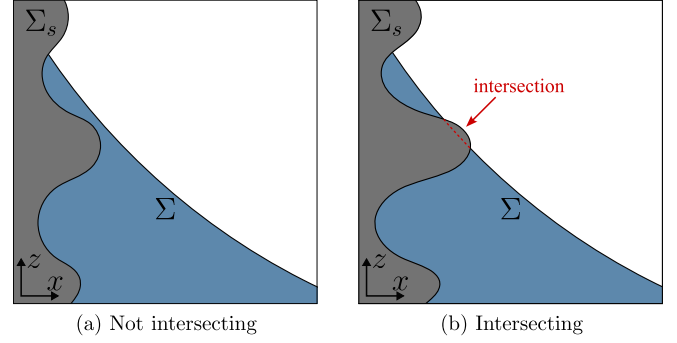


FIG. 3. Schematic illustration of the nonintersection condition and its dependence on the value of R_q . Both (a) not intersecting case with smaller defect amplitude (admissible solution) and (b) intersecting case with bigger defect amplitude (not admissible solution) are shown.

$25 \mu\text{m}$, $R_q = 3 \mu\text{m}$, when $\theta_{\text{eq}} = 75^\circ$ and $a = 2 \text{ mm}$ (shown by thin black solid line) and $a = 5 \text{ mm}$ (shown by bold red solid line). The obtained 3D numerical solutions for the liquid meniscus in the neighborhood of the rough solid plate when $a = 2 \text{ mm}$, and for $i = 250$ and $i = -250$, are shown in Figs. 5(a) and 5(b), correspondingly. Only a part of the rough solid plate enclosed between the planes $z = 500 \mu\text{m}$ and $z = 900 \mu\text{m}$ is shown in Fig. 5. In Fig. 4 the obtained sequence of 750 values of θ_{app}^i , $i = 0, 1, 2, \dots, 750$, is shown for plate displacements $i\Delta$ (withdrawing regime) and $-i\Delta$ (immersing regime), where $\Delta = 2 \mu\text{m}$. The first equilibrium state at $i = 0$ is obtained at the start of the iterative process from a CL height determined by Eq. (7). As one can see from Fig. 4, θ_{app}^i is changing linearly with plate displacement, i.e., $|\theta_{\text{app}}^i - \theta_{\text{app}}^{i+1}| \approx \text{const}$, for $-100 < i < 80$. The vertical dashed lines in Fig. 4 represent the boundaries of the interval $[D^a, D^r]$ where this linear regime is realized. Outside this interval, one can observe a sequence of sharp fluctuations in θ_{app}^i with intermediary sections of linear change with a slope equal

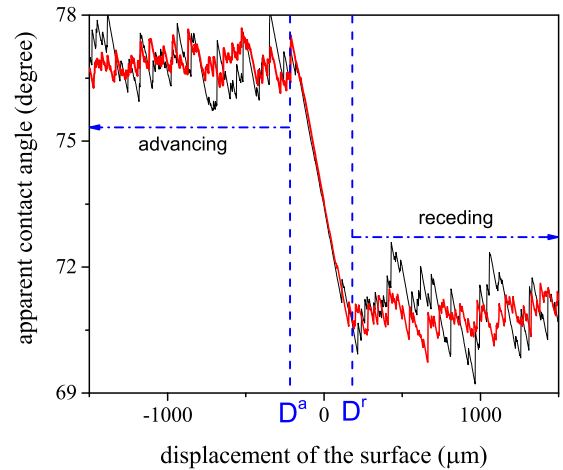


FIG. 4. Apparent CA as function of the plate displacement when $\theta_{\text{eq}} = 75^\circ$ and when the plate surface is characterized by $H = 0.2$, $\lambda_0 = 200 \mu\text{m}$, $\lambda_1 = 25 \mu\text{m}$, $R_q = 3 \mu\text{m}$, and two values of the plate periodicity $a = 2 \text{ mm}$ (thin black solid line) and $a = 5 \text{ mm}$ (bold red solid line).

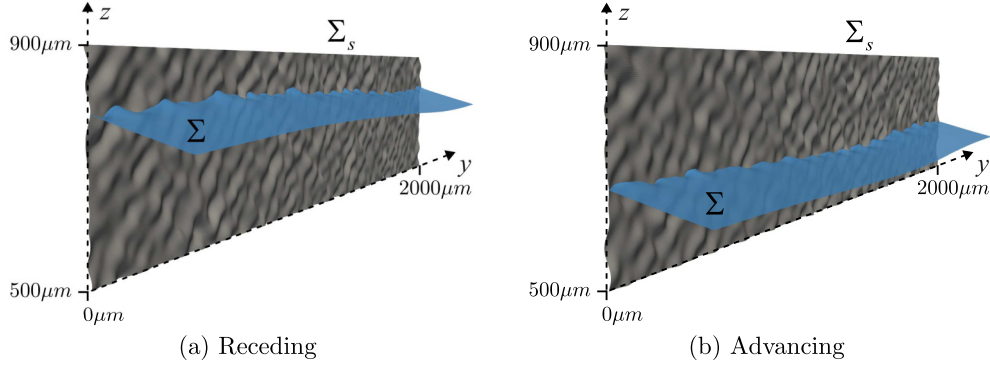


FIG. 5. Numerical solutions for the equilibrium meniscus in the neighborhood of the rough wall when (a) withdrawing the solid plate from the liquid (receding) and (b) immersing the plate in the liquid (advancing).

to the one in the interval $[D^a, D^r]$, resulting in a slip-stick motion. The sharp changes in θ_{app}^i are a direct result of the sudden changes in the CL height [the relationship between θ_{app} and the height $\langle h \rangle$ is determined by Eq. (1) as a result of an avalanche-like process where parts of the CL get detached and move relative to the surface (sliding regime) to reach a new equilibrium state. The RCA θ_r and the ACA θ_a are calculated by averaging θ_{app}^i outside the interval $[D^a, D^r]$ when $i > 80$ and $i < -100$, respectively (in Fig. 4 these areas are marked with arrows). The sections where θ_{app}^i is averaged (they might vary for different system parameters) are determined by the requirement that the averaged value obtained does not change with their further increase. From the results shown for θ_{app}^i one can observe that the amplitude of the fluctuations when $a = 5$ mm are smaller and their frequency is higher than those when $a = 2$ mm. This is due to the fact that the average width of the detached part of L_d in the stick-slip transition of the CL from one equilibrium state to another has a universal characteristic size. Its length, according to the results in Ref. [21], is of the order of $0.4(\lambda_0 + \lambda_1)$. Therefore, as a increases, the ratio L_d/a decreases and hence the fluctuations of the mean CL height $\langle h_i \rangle$ decrease. Smaller fluctuations of $\langle h_i \rangle$, according to Eq. (1), lead to smaller changes in θ_{app}^i . At the same time, at bigger a , more often parts of the CL lose equilibrium and thus fluctuations of $\langle h_i \rangle$ and θ_{app}^i are more frequent. Therefore, increasing a decreases the size of the areas where stable values of the RCA and the ACA are formed. The numerical studies show that for sufficiently big plate displacement Δ , the same ACA or RCA values are achieved over the entire range of values $a \in [1 \text{ mm}, 10 \text{ mm}]$ studied. They do not depend on the size $\Delta_L \leq 2 \mu\text{m}$ of the CL discretization. For definiteness, all the results for the ACA or the RCA presented in the following are obtained for a fixed $a = 5$ mm.

The results for the ACA θ_a and the RCA θ_r as functions of the roughness factor r , for $r < 1.2$, at equilibrium CAs $\theta_{\text{eq}} = 30^\circ, 45^\circ, 60^\circ, 75^\circ$, and 90° are shown in Figs. 6(a)–6(e), respectively. It is important to point out that instead of presenting the dependencies of θ_a and θ_r themselves as functions of the roughness factor r , we prefer to present the dependencies of their cosines on r , since this better illustrates the conclusions drawn from the analysis of the functional dependencies described below. Different discrete values are obtained for $\cos \theta_a$ (solid symbols) and $\cos \theta_r$ (empty symbols) when $R_q = i0.5 \mu\text{m}$, $i = 1, 2, \dots$, and the results for

each set of values of H , λ_0 , and λ_1 are presented by different symbols shown in the legend in each subfigure. The results for $\cos \theta_a$ at $\theta_{\text{eq}} = 90^\circ$ are obtained from the $\cos \theta_r$ results using the *corresponding states* principle. The solid line in the figures show the cosine of Wenzel's angle θ_w . For convenience,

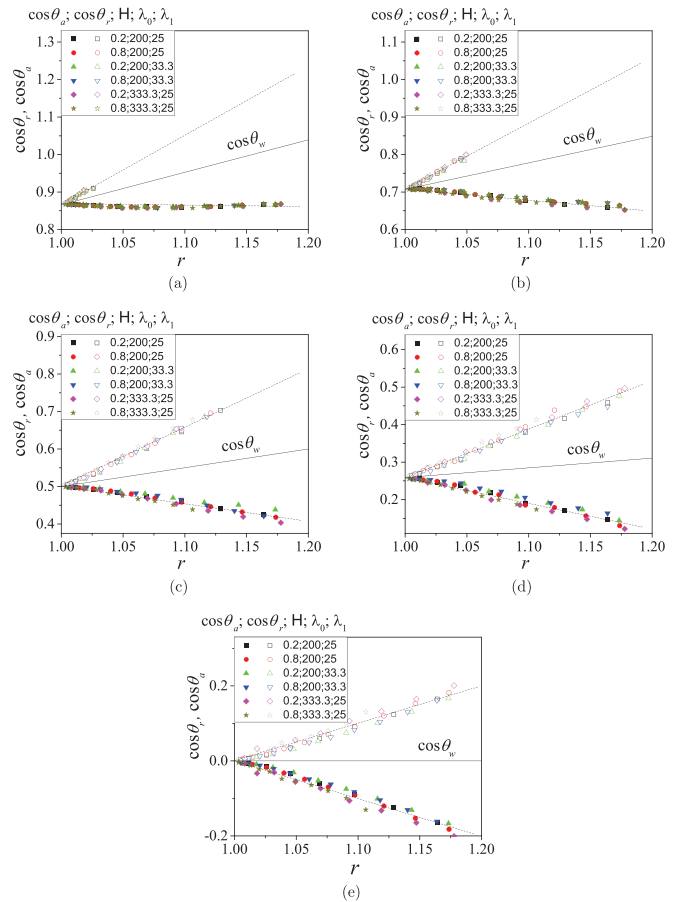


FIG. 6. The cosines of the ACA - $\cos \theta_a$ (solid symbols) and of the RCA - $\cos \theta_r$ (empty symbols) as functions of the surface roughness factor r at different combinations of values of the surface parameters H , λ_0 (in μm), λ_1 (in μm), R_q , and for different values of the equilibrium CAs, which the liquid interface forms with the solid surface: (a) $\theta_{\text{eq}} = 30^\circ$, (b) $\theta_{\text{eq}} = 45^\circ$, (c) $\theta_{\text{eq}} = 60^\circ$, (d) $\theta_{\text{eq}} = 75^\circ$, (e) $\theta_{\text{eq}} = 90^\circ$. The solid lines in all figures show the cosine of Wenzel's angle θ_w .

when comparing the results at different θ_{eq} , the scales on both axes are the same. The dashed lines in the figures show the linear fits of the data. From the results presented in these figures one can conclude that with accuracy up to deviations of the order of $\pm 0.5^\circ$, the $\cos \theta_r$ and $\cos \theta_a$ (and respectively the RCA and ACA) are single-valued functions depending only on the roughness factor r , which is determined by the set of values of H , λ_0 , λ_1 , R_g . The same conclusion, but without taking into account λ_1 , was made by DN for $r \leq 1.0065$ for the linearized energy functional. As one can see from the presented results, $\cos \theta_r$ and $\cos \theta_a$ are well approximated by linear functions of r (while RCA and ACA themselves are well approximated by quadratic functions of r).

The following relation between the functions $\cos \theta_r$ and $\cos \theta_a$ and the cosine of Wenzel's angle holds true:

$$[\cos \theta_r(r) + \cos \theta_a(r)]/2 = \cos \theta_w. \quad (9)$$

A similar relation, but only for $\theta_{\text{eq}} = 90^\circ$, holds true also for the CAs, i.e.,

$$[\theta_r(r) + \theta_a(r)]/2 = \theta_w, \quad (10)$$

which is a result of the corresponding states principle and Eq. (7) when $\theta_w = \theta_{\text{eq}} = 90^\circ$. Taking into account the properties of the cosine function, it follows from (9) that Wenzel's angle is closer to the ACA than to the RCA when $\theta_{\text{eq}} < 90^\circ$. This fact is also noted by DN, even though for the systems studied by them, the CAs $\theta_r(r)$, $\theta_a(r)$, θ_w have very close values due to the small range of considered parameters for which relation (10) holds true in a first-order approximation. Asymmetric behavior of θ_a and θ_r around θ_w is also established experimentally in studies for wetting on rough surfaces (but not self-affine) using abrasive papers [8] and polypropylene surfaces [9]. According to DN, relation (10) is a "result from a free energy that is approximately symmetric about the global minimum θ_w ". However, as one can see from Eq. (6), the free energy depends on the cosine of the CA. Due to that, it is logical that the symmetry of the energy in relation to the global minimum is with respect to the cosine of the CA and relation (9) could be a result of this.

An important characteristic of the wetting properties of the solid surface is the difference of the cosines of RCA and ACA,

$$\cos \theta_r(r) - \cos \theta_a(r), \quad (11)$$

since it is proportional to the adhesive tension [29], the measurable hysteresis force [2], and the maximum receding force [30]. A somewhat unexpected result from the analysis of the obtained results for the $\cos \theta_r$ and $\cos \theta_a$, presented in Figs. 6(a)–6(e), is that at fixed r this difference is a constant, independent of θ_{eq} . This means that for a given material, having a self-affine surface structure, the hysteresis force is the same for all liquids. This property can also be established in the results of Fig. 11 in Ref. [20]. Analyzing the data presented in the figure for the CAH as a function of θ_{eq} , DN noted that the hysteresis increases weakly as the intrinsic CA departs from 90° . Since both $\cos \theta_r$ and $\cos \theta_a$ are well fitted by linear functions of r (as the results in Fig. 5 show), it follows that the CAH $\cos \theta_r - \cos \theta_a$ also has a linear dependence on r . For approximately self-affine rough surfaces, this relation for the CAH was recently confirmed experimentally in Ref. [6] where a correlation between the

CAH and the mean surface height was established. Note that when converting the indicated difference between θ_a and θ_r to a difference of their cosines $\cos \theta_r - \cos \theta_a$, the latter does not depend on the intrinsic CA. The fact that $\cos \theta_r - \cos \theta_a$ does not depend on θ_{eq} is not universally valid just for any rough surface. The analysis of the experimental data [8] (Table 4 there) shows that for rough beeswax surfaces, $\cos \theta_r - \cos \theta_a$ depends on θ_{eq} .

Furthermore, the comparison of the $\cos \theta_r$ and the $\cos \theta_a$ data from Fig. 6 with our results obtained earlier [16] for these angles for doubly periodic smooth rough surfaces, when the kink-depinning regime is realized, reveals that for fixed r the difference $\cos \theta_r - \cos \theta_a$ on self-affine surfaces is much bigger than that on periodic rough surfaces for all θ_{eq} .

IV. CONCLUSIONS

In this paper, we studied numerically the global advancing and receding CAs that occur on random self-affine rough surfaces in Wenzel's wetting regime by using the Wilhelmy plate approach. We propose a framework within which these angles can be unambiguously defined by averaging a large number of realizations of equilibrium CLs of sufficiently long length. In contrast to a previous numerical investigation by DN, performed for a linearized energy functional, leading to strong limitations for the studied roughness factor, we conducted a study for a wide range of roughness factor values by minimizing the full energy functional. We obtained accurate results for the advancing and receding CAs for different plate sizes and different values of the constant local CA. The analysis of the obtained results show that at a fixed local CA, the advancing and receding CAs do not depend directly on individual self-affine surface parameters, but only on the magnitude of the roughness factor. Due to the very small difference between the apparent CAs and the Wenzel's angle in the DN study, the proposed linear relation for the values of these angles cannot be decisively concluded. Instead, our study for larger values of the roughness factor clearly shows that the linear relation holds more generally for the cosines and not the actual CAs. Three main conclusions emerge from our analysis for the cosines of the RCA and the ACA: (1) The dependencies of the cosines of these angles on the surfaces roughness factor are fitted well by linear functions. (2) In agreement with previous studies of rough surfaces, a symmetry between the cosines of the ACA and the RCA relative to the cosine of the Wenzel's angle has been established. (3) Surprisingly, we find that the difference between the cosines of the advancing and receding CAs does not depend on the local CA. Therefore, it follows that on self-affine rough surface all liquids have the same wetting properties, which are determined by the magnitude of the hysteresis force (proportional to the adhesive tension). In contrast to the wetting of doubly periodic rough surfaces, where different depinning mechanisms are observed, in the case of a self-affine rough surface we find that only a kink depinning takes place. Moreover, our studies show that for the same roughness factor, the difference between the advancing and receding CAs is significantly higher for self-affine surfaces than for doubly periodic surfaces in the

kink-depinning regime. The presented numerical results demonstrate how the properties of random self-affine rough surfaces determine their wetting characteristics and the specific relations they follow. It is of interest to further validate experimentally these findings and to perform tests on random as well as regular surfaces in order to establish how

unique they are with respect to different manifestations of surface roughness. More specifically, investigating whether the CAH depends on the local contact angle can be realized by extending the study of Song *et al.* [6] to include various liquids that form different local contact angles with the solid surface.

-
- [1] A. Marmur, C. Della Volpe, S. Siboni, A. Amirfazli, and J. Drelich, *Surf. Innovations* **5**, 3 (2017).
- [2] D. Bonn, J. Eggers, J. Indekeu, J. Meunier, and E. Rolley, *Rev. Mod. Phys.* **81**, 739 (2009).
- [3] D. Quéré, *Annu. Rev. Mater. Res.* **38**, 71 (2008).
- [4] A. Promraksa and L.-J. Chen, *J. Colloid Interface Sci.* **418**, 8 (2014).
- [5] B. N. J. Persson, O. Albohr, U. Tartaglino, A. I. Volokitin, and E. Tosatti, *J. Phys.: Condens. Matter* **17**, R1 (2005).
- [6] Q. Song, K. Liu, W. Sun, Y. Jiao, Z. Wang, X. Liu, and J. Ye, *Phys. Fluids* **34**, 082015 (2022).
- [7] K. Grundke, K. Pöschel, A. Synytska, R. Frenzel, A. Drechsler, M. Nitschke, A. L. Cordeiro, P. Uhlmann, and P. B. Welzel, *Adv. Colloid Interface Sci.* **222**, 350 (2015).
- [8] T. S. Meiron, A. Marmur, and I. S. Saguy, *J. Colloid Interface Sci.* **274**, 637 (2004).
- [9] H. Kamusewitz and W. Possart, *Appl. Phys. A: Mater. Sci. Process* **76**, 899 (2003).
- [10] H. Kamusewitz, W. Possart, and D. Paul, *Colloids Surf., A* **156**, 271 (1999).
- [11] N. Savva, G. A. Pavliotis, and S. Kalliadasis, *J. Fluid Mech.* **672**, 358 (2011).
- [12] G. Palasantzas, and J. T. M. de Hosson, *Acta Mater.* **49**, 3533 (2001).
- [13] R. D. Hazlett, *J. Colloid Interface Sci.* **137**, 527 (1990).
- [14] A. Gauthier, M. Rivetti, J. Teisseire, and E. Barthel, *Phys. Rev. Lett.* **110**, 046101 (2013).
- [15] M. Rivetti, J. Teisseire, and E. Barthel, *Phys. Rev. Lett.* **115**, 016101 (2015).
- [16] S. Iliiev, N. Pesheva, and P. Iliiev, *Phys. Rev. E* **97**, 042801 (2018).
- [17] S. Iliiev, N. Pesheva, and P. Iliiev, *Phys. Rev. E* **101**, 052801 (2020).
- [18] C. Huh and S. G. Mason, *J. Colloid Interface Sci.* **60**, 11 (1977).
- [19] R. G. Cox, *J. Fluid Mech.* **131**, 1 (1983).
- [20] R. David and A. Neumann, *Langmuir* **29**, 4551 (2013).
- [21] P. Iliiev, N. Pesheva, and S. Iliiev, *Phys. Rev. E* **98**, 060801(R) (2018).
- [22] C. Della Volpe, D. Maniglio, M. Morra, and S. Siboni, *Colloids Surf. A* **206**, 47 (2002).
- [23] A. W. Adamson and A. P. Gast, *Physical Chemistry of Surfaces* (Wiley, New York, 1997).
- [24] Y. Yuan, and T. R. Lee, Contact angle and wetting properties, in *Surface Science Techniques*, edited by G. Bracco and B. Holst (Springer, Berlin, 2013), Vol. 51.
- [25] S. Iliiev, N. Pesheva, and V. S. Nikolayev, *Phys. Rev. E* **90**, 012406 (2014).
- [26] S. Iliiev and N. Pesheva, *Phys. Rev. E* **93**, 062801 (2016).
- [27] L. D. Landau and E. M. Lifshitz, *Fluid Mechanics* (Pergamon Press, Oxford, 1987).
- [28] S. Iliiev and N. Pesheva, *J. Colloid Interface Sci.* **301**, 677 (2006).
- [29] S. P. Wesson, Y. K. Kamath, and A. D. Mahale, *Colloids Surf., A* **89**, 133 (1994).
- [30] M. J. Santos, S. Velasco, and J. A. White, *Langmuir* **28**, 11819 (2012).